Materials Science & Engineering A 777 (2020) 139034

Contents lists available at ScienceDirect

Materials Science & Engineering A

journal homepage: http://www.elsevier.com/locate/msea

High cycle fatigue deformation mechanisms of a single phase CrMnFeCoNi high entropy alloy

M. Zare Ghomsheh [a], G. Khatibi [a,*], B. Weiss [b], M. Lederer [a], S. Schwarz [c], A. Steiger-Thirsfeld [c], M.A. Tikhonovsky [d], E.D. Tabachnikova [e], E. Schafler [b]

[a] Institute of Chemical Technologies and Analytics, Christian Doppler Laboratory for Lifetime and Reliability of Interfaces in Complex Multi-Material Electronics, Vienna University of Technology, Getreidemarkt 9/164, A-1060 Vienna, Austria
[b] Physics of Nanostructured Materials, Faculty of Physics, University of Vienna, Boltzmanngasse 5, 1090, Wien, Austria
[c] USTEM, Vienna University of Technology, Austria
[d] National Science Center, Kharkov, Ukraine
[e] B. Verkin Institute for Low Temperature Physics & Engineering, Kharkov, Ukraine

ARTICLE INFO

Keywords:
High entropy alloys (HEAs)
CrMnFeCoNi
Very high cycle fatigue
Failure mechanisms
Dislocations
Twinning

ABSTRACT

High entropy alloys (HEAs) with exceptional mechanical properties have gained a considerable attention in the recent years. Some of these alloys, including the equiatomic, single-phase, face-centered-cubic CrMnFeCoNi alloy with an excellent combination of strength, ductility and fracture toughness at room and cryogenic temperatures have been studied extensively. Still, further studies are required to explain the fatigue behavior and the encountered deformation mechanisms of this class of alloys. In this study, high cycle fatigue behavior of the single-phase CrMnFeCoNi HEA, known as Cantor alloy, has been investigated. S–N curve has been obtained in the range of 10^6 to 10^9 loading cycles by using small-scaled samples and an ultrasonic fatigue test system. Microstructural investigations and fracture surface analyses suggest that cyclic plastic deformation occurs due to the combined interaction of planar slip and deformation twinning at low-stress amplitudes in the very high cycle regime.

1. Introduction

High entropy alloys are a novel class of multi-component metallic materials which are scientifically and technologically interesting and attractive. When the number of constituent elements of an alloy is large, it is possible that the contribution of the configurational entropy to the Gibbs free energy is high enough to suppress the compound formation and phase separation, provided that they are ideal mixtures with random site occupancies [1]. Therefore, these materials have been defined as high entropy [2] or multi-component alloys [3] with near-equiatomic concentrations of 5 or more individual elements. The number of recent studies and review papers show that these new class of compositionally complex alloys have received an increasing interest in the scientific community. HEAs exhibit excellent tensile properties at high and low temperatures, high wear and corrosion resistance and also improved fatigue behavior [4–6]. The prospective application range of these alloys which can be processed as bulk material, coatings and films cover energy, transportation and aerospace sectors [7]. Recently small-scaled HEAs have been suggested as promising materials in Micro-ElectroMechanical Systems (MEMs) and microelectronic devices [8].

Among the wide variety of HEAs, the equiatomic, single-phase, face-centered cubic (FCC) CrMnFeCoNi also known as Cantor alloy, is distinguished due to its excellent properties such as combination of high strength (~1 GPa, even higher in the nanocrystalline state) and ductility (up to 70%), with superior fracture toughness and tensile properties at very low temperatures [3,4,9–11]. These exceptional properties were explained by activation of multiple mechanisms in CrMnFeCoNi HEA during the plastic deformation. It is known that the deformation mechanisms in FCC materials are significantly affected by the stacking fault energy (SFE). At low values of SFE (20–40 mJ/m2), deformation twinning (DT) can be activated resulting in the twinning-induced plasticity (TWIP) effect [12]. Experimental measurements [13] and ab initio calculations [14] report very low SFE values of 18.3–27.3 mJ/m2 and

* Corresponding author.
E-mail addresses: golta.khatibi@tuwien.ac.at (G. Khatibi), martin.lederer@tuwien.ac.at (M. Lederer), sabine.schwarz@tuwien.ac.at (S. Schwarz), andreas.steiger-thirsfeld@tuwien.ac.at (A. Steiger-Thirsfeld), tikhonovsky@kipt.kharkov.ua (M.A. Tikhonovsky), tabachnikova@ilt.kharkov.ua (E.D. Tabachnikova).

https://doi.org/10.1016/j.msea.2020.139034
Received 13 November 2019; Received in revised form 28 January 2020; Accepted 29 January 2020
Available online 30 January 2020

~21 mJ/m2 for the CoCrFeMnNi alloy, respectively. In addition, the ab initio calculations predict a strong temperature dependency of the SFE of this alloy with a strong drop at cryogenic temperatures [14] which might further facilitate the TWIP effect. Besides cryogenic temperatures, the occurrence of deformation twinning has been also related to the amount of strain during the tensile loading. At relatively low strains the planar dislocation glide was found as the dominating deformation mechanism of CrMnFeCoNi HEA whereas at higher strains (~20%) mechanical nano-twinning is additionally activated [9,15]. The remarkable mechanical properties of Cantor at 77K was explained by a transition from planar dislocation slip to mechanical nano-twinning resulting in an increase in the continuous steady strain hardening [4], a decrease in the true strain for the onset of DT and a lower critical stress for twinning which leads to an early formation nano-twins at very low temperatures [10]. DT has also been reported after high pressure torsion severe plastic deformation at room temperature [16], subsequent to rolling [17] and after dynamic loading at high strain rates of up to 104/s [18].

A recent review on the fatigue behavior of different multiphase HEAs mostly obtained under cyclic bending loading conditions reports comparable properties with conventional technical alloys [19,20]. To date, the cyclic response of the single phased CoCrFeMnNi HEAs has been investigated to a very limited extent [21]. Tian et al. [22] studied the fatigue behavior of fully recrystallized bulk ultrafine-grained (UFG) and coarse-grained (CG) CoCrFeMnNi under symmetrical push-pull loading up to 10^7 cycles at 30 Hz. They report an increase of about 40% of fatigue resistance and absence of grain coarsening for the UFG alloy (d~0.65 μm) compared to the CG alloy (d~30 μm) with a fatigue resistance of 200 MPa. The superior fatigue properties of the UFG alloy was related to the fine and recrystallized grain structure, which can intensively accommodate dislocations. Kim et al. [23] studied the role of deformation twins on the tensile and high cycle fatigue behavior of a coarse-grained CoCrFeMnNi HEA (d~245 μm) with a yield and tensile strength of 293 MPa and 625 MPa respectively. They observed a change in the work hardening rate during the tensile deformation which was explained by the dynamic Hall-Petch effect due to twinning. The unexpected cyclic hardening and the high fatigue resistance of ~280 MPa at 10^7 cycles ($R = 0, f = 20$ Hz) were explained by the formation of DTs at stress levels lower than the critical twinning stress in the large-grained material (see also 10a). Thurston et al. [24] studied the effect of temperature on the near-threshold fatigue crack growth rate of CoCrFeMnNi with a grain size of 7 ± 3 μm and a random texture and found an increase of the fatigue threshold value by more than 30% by a decrease in temperature from 293 to 198 K. The increase in ΔK_{th} was explained by the change of the failure mode from transgranular to dominantly intergranular cracking and increase in the strength of the alloy resulting in reduced plastic deformation at the wake of the crack. Cyclic slip as a result of dislocation motion was found as the predominant failure mechanism but not deformation nano-twinning as reported in other studies (e.g. Refs. [25,26]). While the mechanisms of fatigue crack growth and cyclic response of CrMnFeCoNi HEAs have been thoroughly discussed, however, there is an inconsistency between the observed mechanisms of cyclic plastic deformation in these few available studies.

The present work concerns the fatigue response of a single phase CrMnFeCoNi HEA in the very high cycle regime. Fatigue life in the region between 10^5 and 10^9 cycles was determined under symmetrical tension-compression loads allowing a direct comparison with the fatigue properties of a large number of high-performance technical alloys. TEM examination provides further insights into the evolution of dislocation substructure and the encountered mechanisms in relationship with their microstructure and applied cyclic loading conditions.

2. Experimental procedure

2.1. Sample preparation

An equiatomic CrMnFeCoNi alloy was produced by arc melting of pure elements inside a water-cooled copper cavity in high-purity argon. The purities of the alloying elements were ≥99.9%. The ingots were flipped over and re-melted at least 5 times in order to increase chemical homogeneity. Thereafter homogenization high vacuum annealing was carried out at 1000 °C for 24 h. This was followed by rolling deformation and annealing in two steps: a reduction from 5.3 to 2 mm and annealing at 800 °C for 1 h, as well as reduction from 2 to 1 mm and further annealing at 1000 °C for 1 h. The total true strain was ~1.7.

HEAs investigated in the present work was provided as discs with a diameter of 10 mm. Due to the small quantities and limited volume of target material available miniaturized tensile and fatigue samples were designed and cut from the discs by spark erosion. Straight-dumbbell shaped samples with a cross-section of 0.65 mm × 0.4 mm and a gauge length of 2.5 mm were used for tensile tests (Fig. 1a). Fatigue experiments were conducted by using hourglass sample geometry [27] with the dimensions given in Fig. 1b. The rectangular cross-section gauge section of the samples had a width of about 350 μm and a thickness of 200 μm. All the specimens were carefully mechanically polished using P-4000 grit sandpaper (premium SiC abrasive) with water cooling for at least 10 min and then with 0.5 μm alumina polishing suspension with low feed rate to reduce the effect of surface roughness, remove possible damages and to obtain smooth surfaces before tensile and fatigue tests. The dimensions of all samples were measured after the final polishing resulting in an average thickness and width of 206 ± 11 μm and 331 ± 36 μm respectively.

2.2. Microstructural characterization

Microstructural characterization of the CrMnFeCoNi HEA samples was performed by means of optical, scanning and transmission electron microscopy methods (OM, SEM, TEM). The microstructure and grain size distribution of the initial alloy prior and after fatigue testing was characterized with a scanning electron microscope type FEI Quanta 200 FEG by using electron backscatter diffraction (EBSD) technique after metallographic preparation. TEM investigations were conducted by using a transmission electron microscope type FEI Technai F20. In order to investigate the evolution of the substructure after fatigue, few grains with traces of slip marks on the plane surface of the samples were selected. A focused ion beam device type FEI Quanta 200 3D DB-FIB was used to cut out TEM lamellae from these grains. The FIB cuts with an area of about 15 μm × 15μm were prepared after coating of the selected sites with a Pt-protection layer.

2.3. Mechanical properties

To characterize the mechanical properties, nanoindentation techniques and tensile tests were performed on the CrMnFeCoNi samples. The measurements were carried out at room temperature by an ASMEC-Universal Nanomechanical Tester UNAT and using a Vickers indenter. The device was calibrated in terms of indenter stiffness and contact area using fused silica and sapphire standards. About 30 single measurements were performed on each material from which an average value was obtained. Nanoindentation hardness and Young's modulus were determined according to the methods given by Oliver and Pharr [28].

A TA ElectroForce DMA 3200 testing machine (former BOSE) with a load capacity of 450 N and a strain resolution of <0.1% was used to determine the tensile properties of the material. The obtained properties of the samples are listed in Table 1.

High cycle fatigue experiments were performed by using an ultrasonic resonance testing system working at 20 kHz which was adapted for testing of miniaturized samples [27]. A rectangular bar of a high

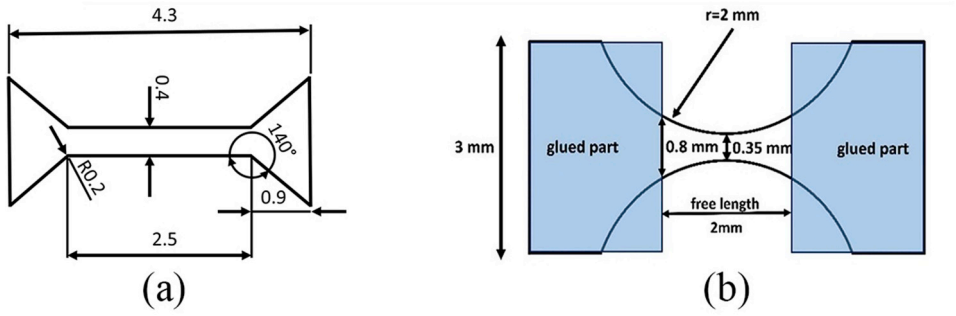

Fig. 1. Schematic of (a) tensile and (b) fatigue samples.

Table 1
Mechanical properties of the CrMnFeCoNi samples.

Young's Modulus [GPa]	H [GPa]	Yield strength [MPa]	Tensile strength [MPa]	Elongation [%]	Fatigue limit at 5e8 MPa	Average Grain Size [μm]
147.7± 4.7	1.54±0.03	262	650	~60	170	45

strength Ti alloy containing a hole with a diameter of 2 mm at its midsection was used as a sample holder. The miniaturized samples were aligned and glued over the hole parallel to the loading direction by using a cyanide-acrylate adhesive. The holder is a part of the fatigue resonance testing system which is excited to longitudinal push-pull vibration with zero mean stress (R = −1) (Fig. 2a). During the entire loading, a video camera attached to a light microscope was used to monitor the plane surface of the specimens and to determine the time to fracture. The tests were performed at room temperature with additional cooling of the specimen by pressurized dry air. A schematic of the fatigue testing set-up is presented in Fig. 2a and more details are given in Ref. [27].

The stress amplitude was calculated based on the experimental strain calibrations and Finite Element Analysis (FEA) which was performed by using ANSYS software. Miniature strain gauges were applied on the midsection of the holder at its side face and on the plane surface of a calibration sample with a width of ~689 μm and a thickness of 205 μm. The strain amplitude $\left(\frac{\Delta\varepsilon}{2}\right)$ of the holder and the sample was measured at several levels to determine their strain ratio, $R_E = \frac{\Delta\varepsilon_{sample}}{\Delta\varepsilon_{holder}}$ (Fig. 3). Under the assumption of preliminarily elastic deformation of the specimen at the VHCF region, the actual stress amplitude of the samples during the testing can be determined according to Eq (1a):

$$\frac{\Delta\sigma}{2} = R_E . K_t . E . \left(\frac{\Delta\varepsilon}{2}\right)_{holder} \quad (1a)$$

where E is the elastic modulus of the sample, R_E is the experimentally

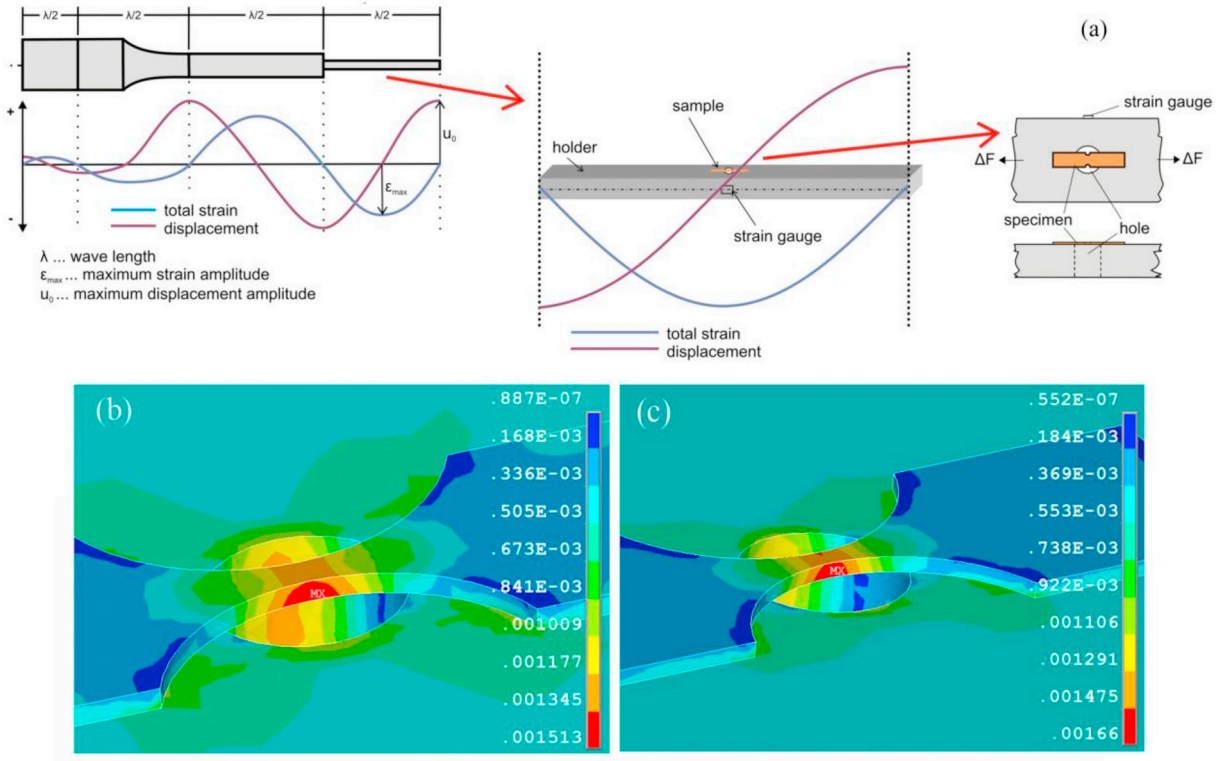

Fig. 2. Schematic of ultrasonic fatigue testing system and experimental set up for miniaturized specimens (a), plots of strain distribution for two hourglass samples with cross sections of 370 x 220 μm^2 (b) and 285 x 190 μm^2 (c) for a strain amplitude of 4.2e-4 at holder (b, c).

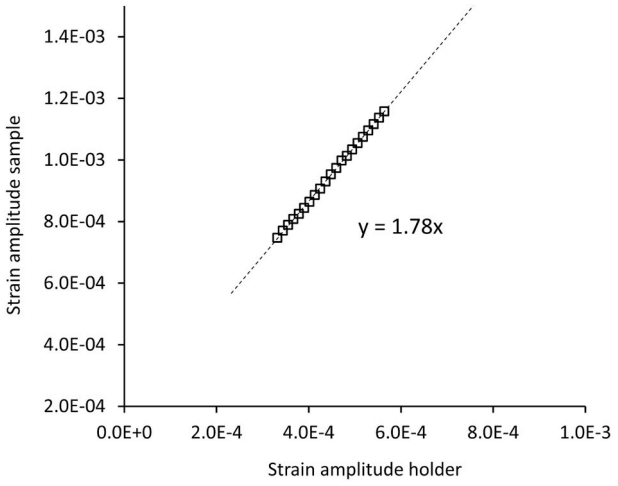

Fig. 3. Calibration curve for determination of strain in the miniaturized samples.

determined strain ratio, K_t is the theoretical net stress concentration factor of the hourglass samples, $\left(\frac{\Delta\varepsilon}{2}\right)_{holder}$ is the strain of the specimen holder [27].

Examples of strain distribution plots for two hourglass fatigue samples which are mounted across the hole on the specimen holder are presented in Fig. 2b and c. Simulations revealed that the value of the strain component ε_{yy}, along the y-axis of sample and holder was nearly identical with the value of von Mises strain. Furthermore, a gradient of strain is observed in the gauge section with a gradual decrease across the thickness from the lower to the upper surface of the sample. The calculated stress concentration factor $K_{t\text{-}FEM}$ which corresponds to the ratio of the strain at the location of highest stress concentration at the side faces of the samples to the sample holder was determined by considering the geometrical variations of the miniaturized samples. The difference between the cross-sections of the samples (~0.054–0.081 μm^2) resulted in $K_{t\text{-}FEM}$ values in the range of 3.6–3.9 with a variation of ~9%. Considering that the experimental calibration curve was determined for one geometry, the calculated $K_{t\text{-}FEM}$ values were used for determination of the stress amplitude by using Eq (1b):

$$\frac{\Delta\sigma}{2} = K_{t-FEM}.E.\left(\frac{\Delta\varepsilon}{2}\right)_{holder} \quad (1b)$$

3. Results and discussion

3.1. Microstructure

The EDX analysis and elemental mapping resulted in a homogeneous distribution of the elements with a composition of Cr, Mn, Fe, Co and Ni are 19, 19, 20, 21 and 21 at. % respectively (Fig. 4a). The microstructure of the CoCrFeMnNi HEA exhibits a typical single-phase FCC structure with random orientation and a high amount of annealing twins (Fig. 4b). The grain size distribution plot (Fig. 4c) reveals that annealing at 1000 °C for 1 h resulted in coarsening of the recrystallized grains as well as partial grain growth with a mean grain diameter of ~45 μm. Occasionally Cr–Mn- rich oxide particles with diameters in the range 0.5 to about 2 μm were observed as exemplary shown Fig. 4d. TEM investigations showed occasionally such particles.

Engineering and true stress-strain curves of the CrMnFeCoNi samples at a strain rate of $10^{-3}s^{-1}$ and room temperature are shown in Fig. 5 a. which is typical for FCC materials with pronounced plasticity. Fig. 5 b. shows a true stress-strain curve and corresponding strain hardening rate ($d\sigma/d\varepsilon$) curve as a function of strain. In the region of low strains (I) a rapid decrease in the strain hardening rate is observed which is followed by a rather constant hardening rate (II) up to about 0.2 of deformation, above which again a gradual drop of the curve is observed (III). The three regions of the strain hardening curve can be related to different deformation mechanisms. The dominant tensile deformation at stage I which correspond to low plastic strains is planar dislocation slip. The change in the hardening rate in the region II is related to the additional effect of deformation twinning acting as barriers against the dislocation movement which is also known as the dynamic Hall–Petch effect. The drop of the strain hardening rate at high plastic strains has been related to the saturation of the twinning activation resulting in a dislocation slip controlled plastic deformation [25].

The single-phase CrMnFeCoNi alloy displays ultimate tensile strength levels of 650 MPa and excellent ductility (60%), which is similar to the mechanical properties obtained in other studies [5,23,25]. In all specimens, yielding and subsequent flow occurs smoothly without any discontinuities such as yield drops or serrated flow. The uniaxial tensile properties, Young's modulus and nano-hardness of the alloy together with average grain size obtained by SEM Electron Backscatter Diffraction (EBSD) are given in Table 1.

3.2. Fatigue life curves

The S–N curve of hourglass shaped CrMnFeCoNi samples is shown in Fig. 6 revealing results between 230 MPa at $N = 10^6$ and an endurance limit of about 160 MPa at 10^9 cycles. The data shows a relative high scatter which might be due to the small size of samples and the possible presence of different defects in the alloy as also reported in other studies [20]. Occasionally inclusions which were identified as Mn–Cr-rich oxides and small pores were found on the fracture surfaces of fatigued samples. These can act as stress concentration sites and result in an earlier failure and scatter of data. It has been suggested that the HEAs such as CrMnFeCoNi, providing excellent properties have the potential to be material for stent implant applications if pores and cast defects are eliminated [29,30].

A first approach to discuss the technical applicability of new alloys under cyclic loading conditions is to evaluate the relation between fatigue endurance strength (S_d) at $N = 10^7$ to the ultimate tensile strength (σ_{UTS}) is given by $S_d = 0.5\sigma_{UTS}$ (see also Ashby plots [26,31,32]). Using this ratio, Tang et al. [26] made a comparison of the fatigue data obtained for selected technical alloys with HEAs and found a linear relation described by $S_d = k.\ \sigma_{UTS}$, with k being the fatigue ratio which is in the range between 0.18 up to 0.35. A similar analysis was performed in this study as presented in Fig. 7. This plot comprises only the fatigue data obtained under axial loading at a stress ratio of $R = -1$ in order to exclude the effect of loading conditions. However, the testing frequency varies between the conventional frequencies of ≤200 Hz up to ultrasonic frequencies of 20 kHz.

The gathered data are bound between a higher and a lower boundary with k values of ~0.5 and ~0.28 with the highest values corresponding to materials such as Ti alloys and high-performance steels. In spite of the difference between the sample dimensions and their grain size, the fatigue ratios ($k = S_d/\sigma_{UTS}$) of the bulk equiatomic CrMnFeCoNi high entropy alloys reported by Tian et al. [22] comply very well with our data with a k~0.28 at $N = 10^7$. They found values of 0.28–0.32 for the coarse- and fine-grained samples with GS of 30 μm and 0.65 μm respectively [22]. A higher ratio of k~0.44 was obtained by Kim et al. [23] for a large grained material with an average grain size of 245 μm. HEAs are in the intermediate region.

Since the high cycle fatigue experiments of the present study were conducted at ultrasonic frequencies, a brief review of the studies on the frequency effect on the fatigue response of metals is given. It has been reported that the effect of ultrasonic testing frequency on high cycle fatigue behavior of technical alloys at low stress levels is not significant [33]. In a study by Bajons et al. [34] lifetime of different metals and technical alloys were compared at the testing frequencies of 200 Hz and 20 kHz in the range of 10^4 to ~10^8. A change in the lifetime of 316 and

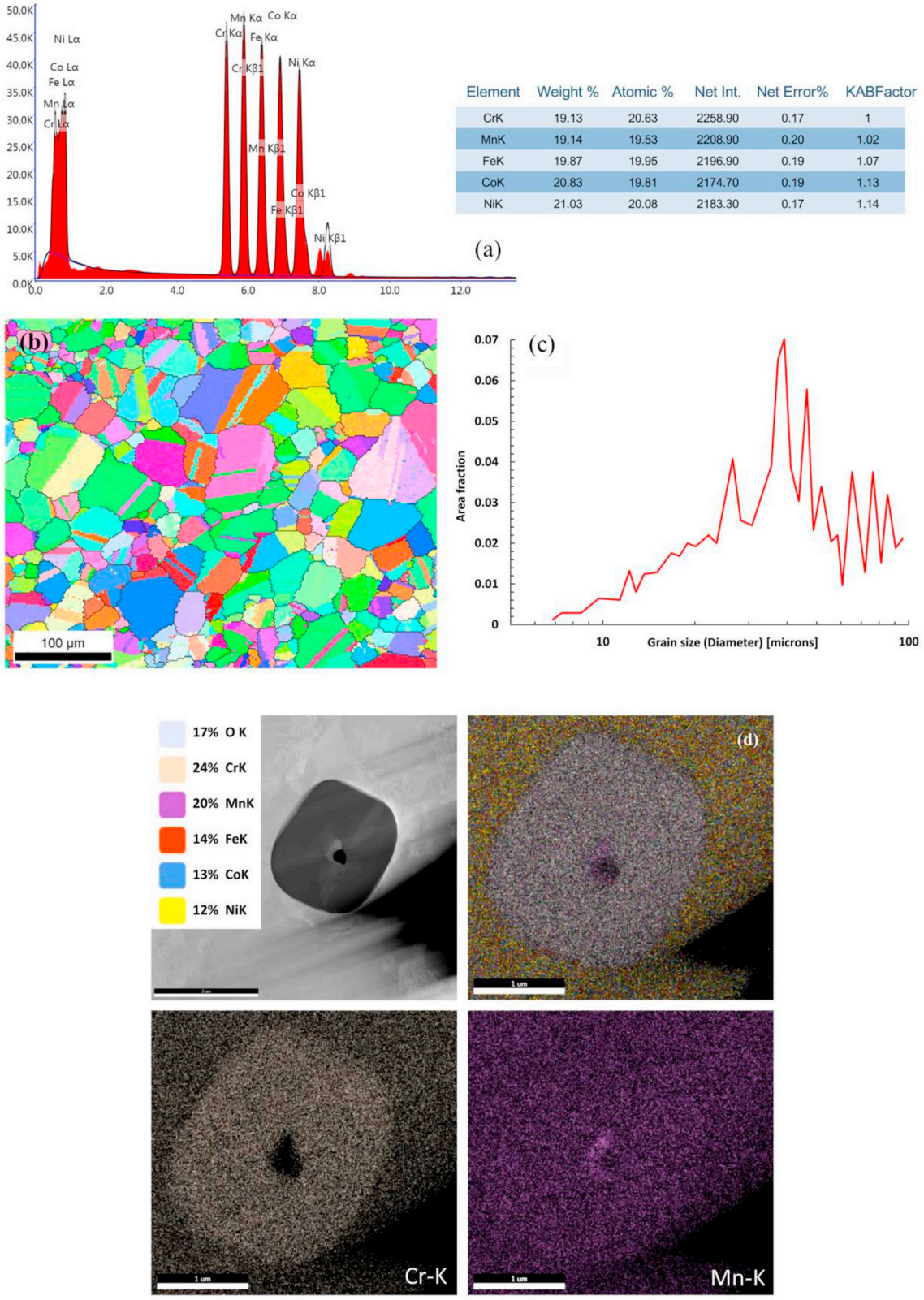

Element	Weight %	Atomic %	Net Int.	Net Error%	KABFactor
CrK	19.13	20.63	2258.90	0.17	1
MnK	19.14	19.53	2208.90	0.20	1.02
FeK	19.87	19.95	2196.90	0.19	1.07
CoK	20.83	19.81	2174.70	0.19	1.13
NiK	21.03	20.08	2183.30	0.17	1.14

Fig. 4. EDX spectrum (a) EBSD grain orientation map (b) grain size distribution plot (c) and STEM HAADF image of a Cr–Mn- rich oxide particle with the corresponding EDS mapping images (d) of CoCrFeMnNi HEA.

X3CrNi134 steels at 10^8 at ultrasonic frequency was not found. In the case of pure FCC metals, fatigue resistance of Cu increased only about 10% while a much pronounced effect was reported for soft Al with an increase of ~50% [34]. In the case of BCC (base centered cubic) metals and alloys, the majority of the fatigue studies confirm that high frequency testing results in a prolonged lifetime [34–37]. The frequency effect or cyclic strain rate dependency has been principally attributed to the crystal structure and accordingly to the thermally activated

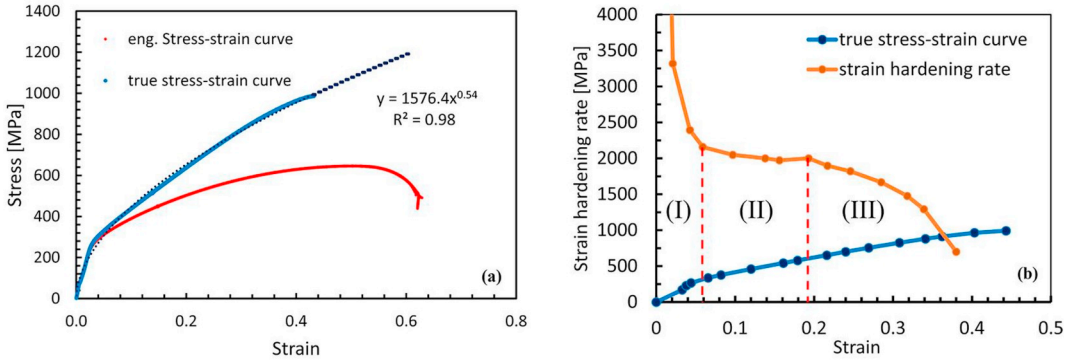

Fig. 5. Engineering and true stress-strain curves (a) and the strain hardening rate curve (b) of the equiatomic CrMnFeCoNi HEA at a strain rate of $10^{-3}s^{-1}$ and at room temperature.

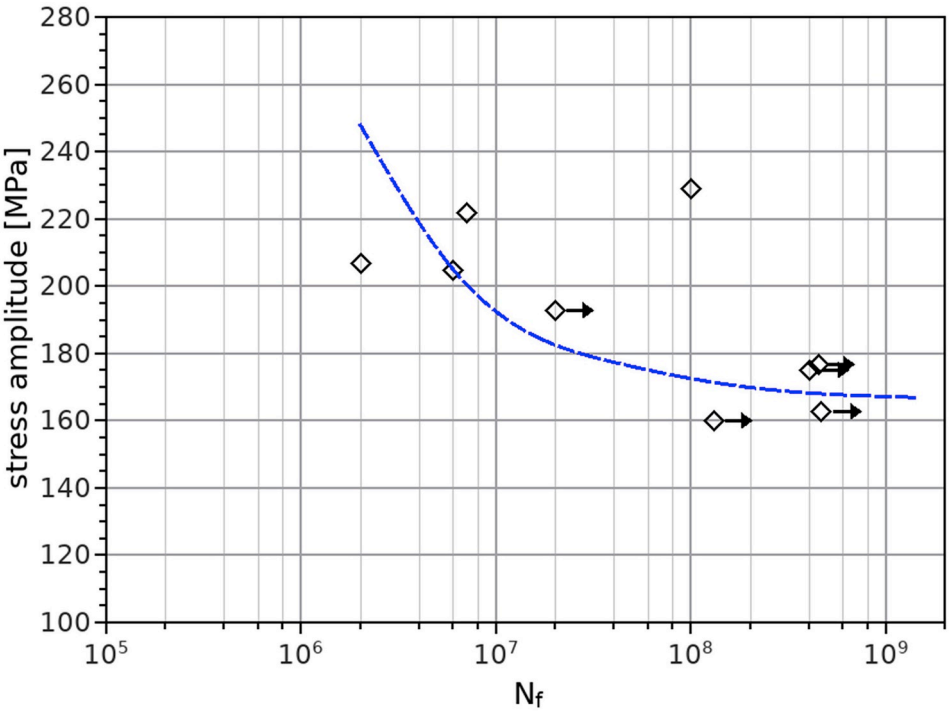

Fig. 6. Fatigue life curve of hourglass shaped CrMnFeCoNi samples (test conditions: 20 kHz, R = −1 and RT).

dislocation motion in the metallic materials. In BCC metals, the dislocation motion associated with high lattice friction and high activation energy exhibits a strong deformation rate dependency. This effect was found to be less significant in materials with a FCC structure [38]. A quantitative comparison of the fatigue life at conventional and ultrasonic testing frequencies for the HEA alloy of this study is not available. However above considerations and a comparison with the available data (Fig. 7), suggests a moderate or low frequency effect for CrMnFeCoNi alloy.

3.3. Microstructural investigations

A typical crack growth path on the plane surface of a CoCrFeMnNi sample after fatigue failure at a stress amplitude of 222 MPa and $N_f = 7 \times 10^6$ is shown in Fig. 8a. The corresponding EBSD image which was prepared after polishing the sample surface is given together with the grain size distribution plot in Fig. 8b. Cracks were mainly initiated from one of the sample corners and propagated along a crystallographic path in a predominant transgranular manner through the grains and along the slip lines. Occasionally, intergranular cracking along some of the grain boundaries was found as can be observed on the bifurcated crack in Fig. 8a. Slip marks are observed at the surface of the single grains at both sides of the main crack similar to those observed in FCC metals such as Cu. Traces of {111} planes are identified on the marked grains on which slip marks are observed (Fig. 8b). Backscattered Electrons (BSE) image of the polished surface of a sample in the vicinity of fatigue crack reveals a microstructure with a high dislocation density and a large number of parallel micro-bands within one of the grains which are attributed to deformation twins (Fig. 9a and b).

Deformation twinning has been recognized as the pre-dominant deformation mechanism of HEAs during tensile loading and high plastic strains [21]. Concerning the fatigue loading contradictory results have been reported [23,24,50]. Our observations indicate that deformation twinning in CoCrFeMnNi HEA can be promoted at very high loading cycles. These will be discussed in more details in the next section.

The fatigue fracture surface of CrFeNiMn HEA samples complied well with the crack path observed on their plane surface. The fracture surface with a rough morphology reveals a dominant transgranular failure mode with a number of facetted grains indicating that failure also occurred to

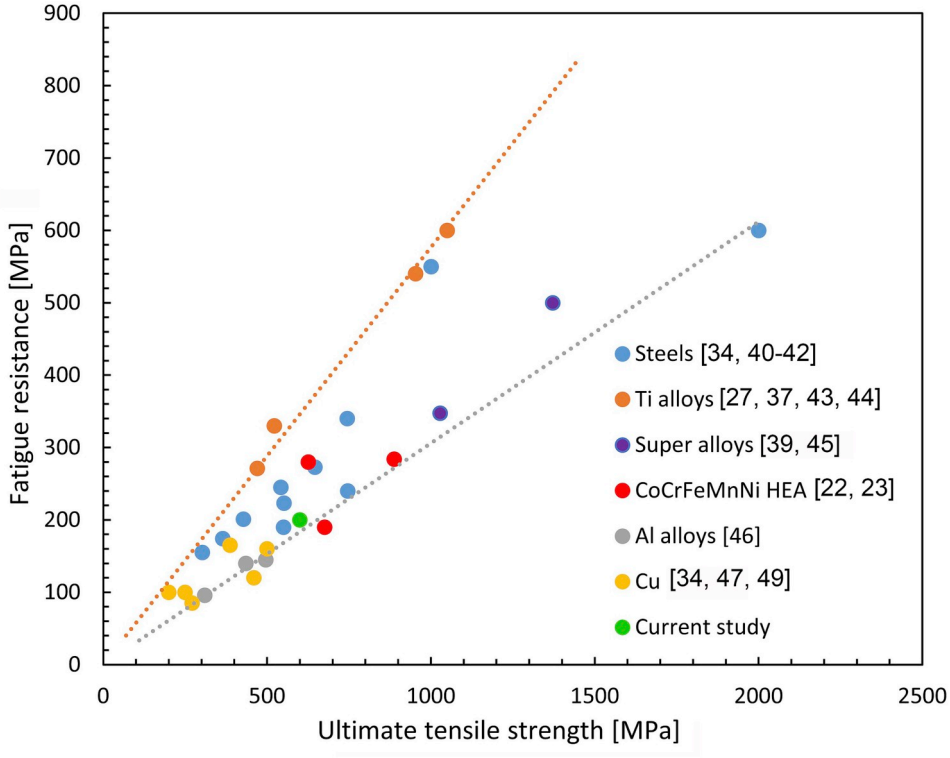

Fig. 7. Relationship between the tensile strength and fatigue strength of a number of technical alloys with Cantor at N = 10^7 and R = −1 at different testing frequencies. Steels [34,40–42], Ti alloys [27,37,43,44], Super alloys [39,45], CoCrFeMnNi HEAs [22,23], Al alloys [46], Cu alloys [34,47–49].

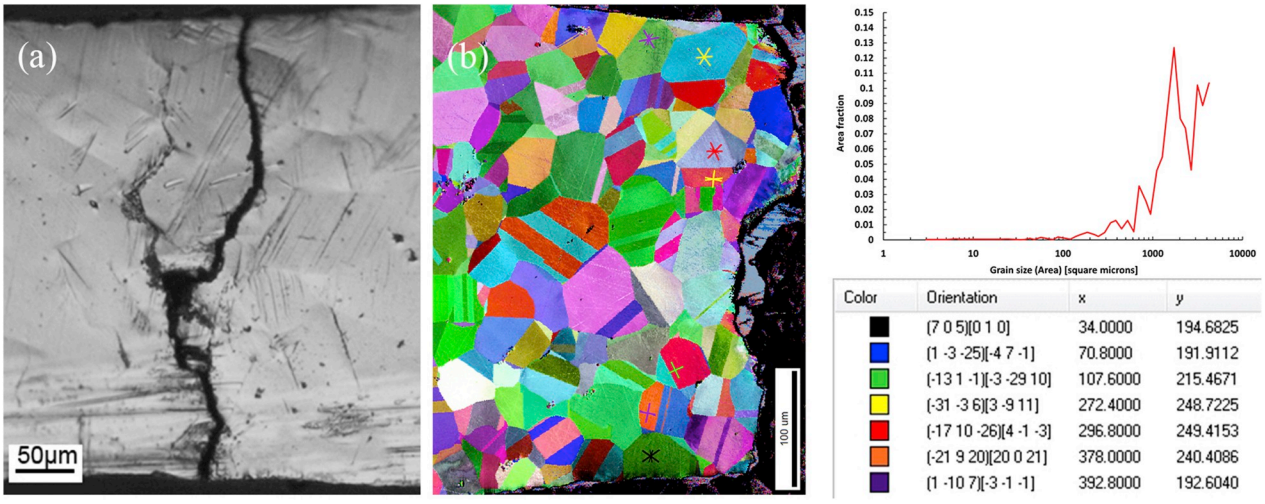

Fig. 8. Crack path on the surface of a failed sample, with bifurcation after fatigue at $\Delta\sigma/2 = 222$ MPa and $N_f = 7 \times 10^6$ (a), IPF PRIAS image of the cracked sample, marked grains show traces of [111] plane (b).

some extent due to intergranular cracking or possibly along the slip planes (Fig. 10a–d). The surfaces of the majority of grains display slip steps and striation which were formed as a result of planar slip during cyclic loading [24]. Furthermore, few inclusions and small pores are embedded within the fractured grains. Pores and occasionally polyhedral indents are also found on the facetted grains which indicates grain boundary porosity in the alloy. The indents have been observed also in Ref. [24] and suggested to be ends of recrystallization twins which were formed perpendicular to the grain boundaries during the processing of the alloy. The fine parallel protrusions are shown on a facet in Fig. 10d can be interpreted as traces of deformation twins on the grain boundaries (10c, d). Similar features were observed in TWIP steels which were reported as secondary cracks along the slip-line traces indicating a tendency to slip band type cracking [51].

The TEM investigations of the CrMnFeCoNi samples after failure revealed the formation of two types of distinct substructures suggesting two different deformation mechanisms in the high cycle regime (Fig. 11a –d). Fig. 11a and b shows an overview of the region in the vicinity of the failure site with a considerable amount of DTs. Fig. 11c which corresponds to the area next to the fracture surface shows a microstructure consisting of dislocation cells and bundles of deformation twins. The cell structure consisting of rather thick walls surrounding the dislocation free region resembles those commonly observed in FCC metals subjected to fatigue and displays an average cell size of about

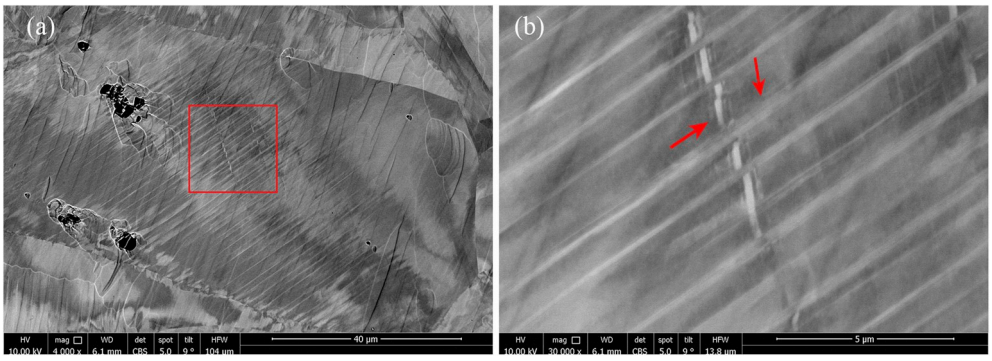

Fig. 9. BSE images of highly deformed grains of a fatigued sample $\Delta\sigma/2 = 229$ MPa and $N_f = 1 \times 10^8$ in the vicinity of the fatigue crack (a), with detail showing the intersection of deformation twins (b).

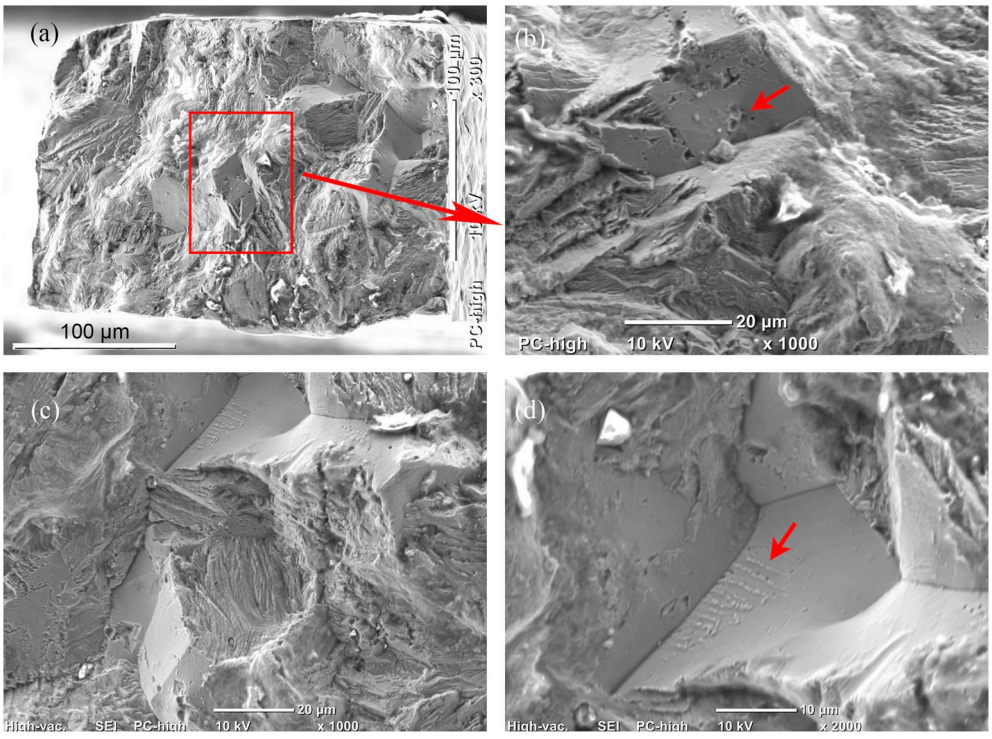

Fig. 10. Overview of the fatigue fracture surface of a CrMnFeCoNi sample after failure at 193 MPa and $N_f = 3.1 \times 10^7$ (a) and details showing cleavage steps and plane faceted grains with pores (b) regions of *trans*- and inter-granular fracture paths (c) and traces of deformation twins on a cleaved facet (d).

500 nm in this region (Fig. 11d). Deformation twins which were found as a number of parallel bundles (Fig. 11e) or partial segments (Fig. 11d) correspond very well to the BSE images presented in Fig. 9.

Examination of the samples revealed the presence of a high-volume fraction of deformation twins in the area close to the failure site in the midsection of a sample with a gradual reduction further away from this area. The thickness of the twins which contained a high dislocation density was found to be in the range of about 80–150 nm. The distribution of the elements in the twinned region remained homogeneous as examined by EDS mapping (Fig. 12).

Formation of a dislocation substructure with rather thick deformation twins has also been observed by Ref. [52] during cold rolling of CrMnFeCoNi HEAs. It is interesting to note that very similar bundles of thick parallel deformation twins as shown in Fig. 10 have been observed in a study on the evolution of adiabatic shear localization in austenitic stainless steel subjected to high strain rate dynamic loading [53]. It was found that these types of twins were formed within the shear bands prior to the large deformation during the Hopkinson experiments. The similarity of the observed features may indicate that the evolution of this specific DT substructure as a result of cyclic plastic deformation of the CrMnFeCoNi samples at rather low strain amplitudes in high cycle regime, might be further facilitated by the prevailing conditions during the ultrasonic fatigue experiments. In a study by Li et al. [18] ballistic properties of CrMnFeCoNi HEA with a mean grain size < 10 µm were investigated using the same method described in Ref. [53]. The authors observed an equiaxed ultrafine-grained microstructure within the adiabatic shear bands which have been formed as a result of significant dynamic recrystallization. Contrary to Ref. [53], deformation twinning was not found in this case which might be related to the small grain size of the tested HEA samples. It is known that twinning becomes more difficult with decreasing the grain size [21].

The role of twinning on the failure mechanism has been subject of a number of studies on fatigue behavior of TWIP steels [51,54,55]. In a study by Roa et al. [54], intensive formation of DTs which were preferably formed in the grains with a crystallographic orientation close to (111) plane was related to the increase in dislocation density during the

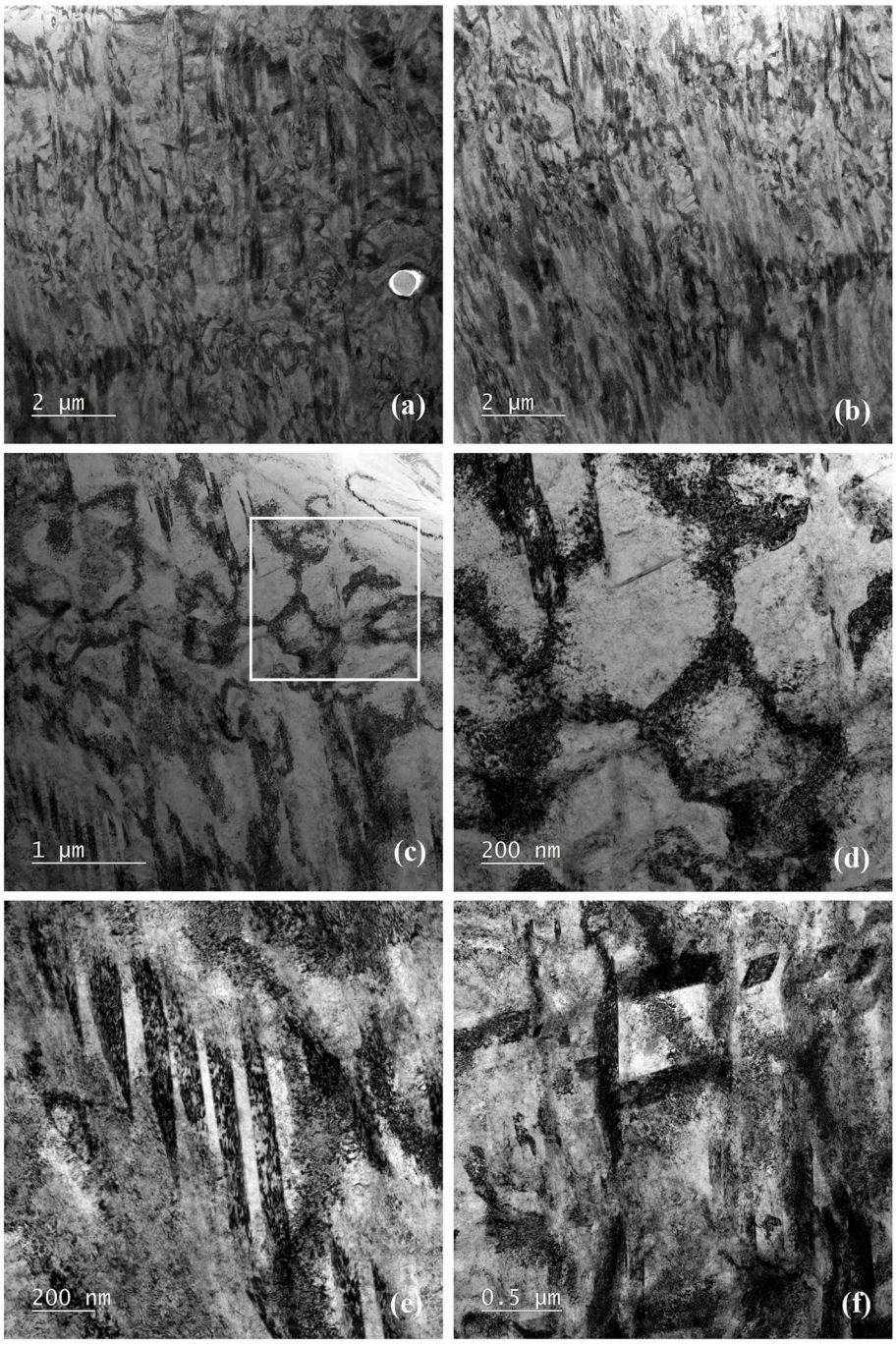

Fig. 11. BF-TEM image of CrMnFeCoNi sample after fatigue failure showing an overview of the substructure in the vicinity of fracture surface (a, b), dislocation cells and DTs (c), details of dislocation cell structure shown in c (d), regions containing bundles of parallel thick deformation twins (e) and intersecting twins (secondary twinning) (f).

high cycle fatigue loading. The damage mechanism was mainly attributed to the high stress concentration generated during the growing of first order twins and nucleation of serrated micro-cracks at the grain boundaries. Hamada et al. [51] reported on initiation fatigue cracks at early stages of loading of high Mn TWIP steels. Favorable crack initiation sites were found to be the intersections of slip bands, grain boundaries and annealing twin boundaries. However, deformation twinning or phase transformation was not observed. In a further study, presence of large grains was found to promote deformation twinning. Early initiation of micro-cracks during the loading followed by a low propagation rate at higher cycles in fine grained material, contributed to enhanced fatigue resistance in TWIP steels [55].

The few available studies on the microstructural evolution of CrMnFeCoNi subjected to cyclic fatigue are not consistent. Tian et al. [22] did not find a specific dislocation substructure in the UFG CrMnFeCoNi. The absence of a cell structure was explained by the small size of grains, whereas the absence of DTs was attributed to an increase in the twinning stress due to grain refinement. Kim et al. studied the fatigue properties of a coarse-grained CrMnFeCoNi alloy with d~250 μm and observed fatigue crack propagation along the boundaries of the twins which have been formed during the cyclic loading. They suggested that formation of DTs contributes to the enhancement of fatigue resistance in the high cycle regime [23]. The difference between the fatigue induced substructure and the encountered mechanism reported in these

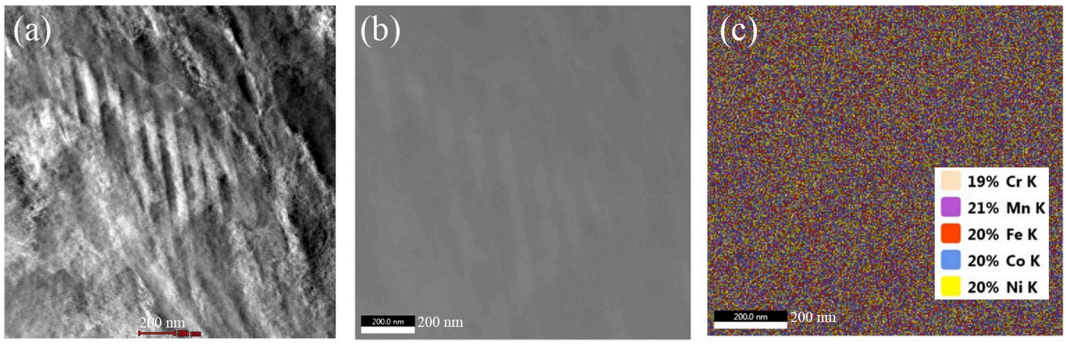

Fig. 12. STEM-BF image (a) and HAADF−STEM image of the CoCrFeMnNi HEA with DTs (b), the corresponding EDS mapping image of the same sample area showing a homogeneous distribution of all elements (c).

studies is most probably related to the grain size of the fatigue samples which vary from few microns to ~250 μm. The dependency of the microstructure and the dominating deformation mechanism of the HEAs during quasi-static loading has been subjected to a number of investigations [50,56,57]. In a study by Sun et al. [50] a dependency between the maximum flow stress, the predicated twinning stress and the grain size of CrMnFeCoNi HEA was found by using the following equation for calculation of the twinning stress (σ_{tw}):

$$\sigma_{tw} = m\frac{\gamma}{b_p} + \frac{k_{tw}}{\sqrt{d}} \quad (2)$$

The twinning stress was obtained with a Taylor factor (m) of 3.06, SFE (γ) of 21 mJ/m^2, the Burgers vector of a partial dislocation (b_p) of 1.46 × 10^{-10} m, the Hall–Petch constant for twinning (k_{tw}) of 980 MPa μm$^{1/2}$ and (d) the grain size of different samples. It was suggested that the deformation twinning is first activated when the grain size exceeds ~3 μm (twinning stress ~1000 MPa). Accordingly, for the CrMnFeCoNi sample of this study with an average grain size of ~45 μm the critical twinning stress during the tensile loading is expected to be about 580 MPa. Considering the SFE values of 18–25 mJ/m^2 and b_p of 1.49 × 10^{-10}m as given in Ref. [13], the approximated twinning stress varies in the range of ~350–650 MPa.

The mechanisms of fatigue in metallic materials differ substantially from those occurring during the monotonic loading, however, a qualitatively similar dependency on the grain size can be postulated. While cyclic slip and DTs may compete with each during cyclic loading, the dominant mechanism would not only be dependent on the applied stress amplitude and loading cycles but also on the grain size and texture of the CrMnFeCoNi HEAs.

4. Conclusion

In this work, cyclic deformation behavior of CoCrFeMnNi high entropy alloy after very high cycle fatigue was studied. The focus was on understanding the mechanism of cyclic plastic deformation of CoCrFeMnNi by means of microstructural analysis as summarized below:

- The single phased FCC solid solution alloy revealed a mean grain diameter of ~45 μm and a proportion of large grains of ~100 μm. The material contained a small number of pores and Cr–Mn oxides with a particle size ≤2 μm. The yield and tensile strength were 262 MPa and 650 MPa respectively.
- S–N curve has been obtained in the range of 10^6 to 10^9 loading cycles by using an ultrasonic fatigue test system with a fatigue resistance of 180 MPa at 10^7 and endurance limit of 160 MPa at 10^9.
- The applied ultrasonic testing method provides the possibility to study the fatigue behavior of small-scaled specimens under symmetrical tensile loading up to very high cycle regime.
- TEM examination of the fatigued samples reveal that dislocation slip and deformation twinning both contribute to cyclic plastic deformation at low strain amplitudes in the high cycle regime
- It was found that deformation twinning can occur at room temperature and relative low stresses below the nominal critical stress for twinning in CoCrFeMnNi HEA after a high number of loading cycles.
- The results of microstructural investigations suggest that the evolution of DT during the cyclic loading at room temperature is strongly dependent on the grain size.
- The relationship between the tensile properties and high cycle fatigue resistance of CoCrFeMnNi HEA were found to be comparable with those of high-performance technical alloys and suggests a broad application field for this material including energy, transportation, and aerospace to microelectronics sectors.

Declaration of competing interest

The authors declare that they have no known competing financial interests or personal relationships that could have appeared to influence the work reported in this paper.

CRediT authorship contribution statement

M. Zare Ghomsheh: Formal analysis, Data curation, Writing - original draft. **G. Khatibi:** Investigation, Supervision, Writing - original draft, Funding acquisition. **B. Weiss:** Supervision, Writing - original draft. **M. Lederer:** Formal analysis. **S. Schwarz:** Investigation. **A. Steiger-Thirsfeld:** Investigation. **M.A. Tikhonovsky:** Resources. **E.D. Tabachnikova:** Resources. **E. Schafler:** Supervision, Writing - original draft, Funding acquisition.

Acknowledgments

We are grateful to M.A. Tikhonovsky from Kharkov Institute of Physics and Technology and E.D. Tabachnikova from B. Verkin Institute for Low Temperature Physics, Kharkov, Ukraine for conducting the alloying, M. Lederer from CD Laboratory / CTA for FEM, S. Schwarz and A. Steiger-Thirsfeld from USTEM, TU Wien for TEM and EBSD images. The financial support by the Austrian Federal Ministry for Digital and Economic Affairs and the National Foundation for Research, Technology and Development is gratefully acknowledged.

References

[1] N.L. Okamoto, S. Fujimoto, Y. Kambara, M. Kawamura, Z.M. Chen, H. Matsunoshita, K. Tanaka, H. Inui, E.P. George, Size effect, critical resolved shear stress, stacking fault energy, and solid solution strengthening in the CrMnFeCoNi high-entropy alloy, Sci. Rep. 6 (2016) 35863.

[2] J.W. Yeh, S.K. Chen, S.J. Lin, J.Y. Gan, T.-S. Chin, T.T. Shun, C.H. Tsau, S.Y. Chang, "Nanostructured high-entropy alloys with multiple principal elements: novel alloy design concepts and outcomes, Adv. Eng. Mater. 6 (5) (2004) 299–303.

[3] B. Cantor, I.T.H. Chang, P. Knight, A.J.B. Vincent, Microstructural development in equiatomic multicomponent alloys, Mater. Sci. Eng., A 375 (2004) 213–218.
[4] B. Gludovatz, A. Hohenwarter, D. Catoor, E.H. Chang, E.P. George, R.O. Ritchie, A fracture-resistant high-entropy alloy for cryogenic applications, Science 345 (6201) (2014) 1153–1158.
[5] F. Otto, A. Dlouhý, C. Somsen, H. Bei, G. Eggeler, E.P. George, The influences of temperature and microstructure on the tensile properties of a CoCrFeMnNi high-entropy alloy, Acta Mater. 61 (15) (2013) 5743–5755.
[6] A. Gali, E.P. George, Tensile properties of high- and medium-entropy alloys, Intermetallics 39 (2013) 74–78.
[7] D.B. Miracle, J.D. Miller, O.N. Senkov, C. Woodward, M.D. Uchic, J. Tiley, Exploration and development of high entropy alloys for structural applications, Entropy 16 (1) (2014) 494–525.
[8] Y. Zou, H. Ma, R. Spolenak, Ultrastrong ductile and stable high-entropy alloys at small scales, Nat. Commun. 6 (1) (2015) 1–8.
[9] B. Gludovatz, E.P. George, R.O. Ritchie, Processing, microstructure and mechanical properties of the CrMnFeCoNi high-entropy alloy, JOM (J. Occup. Med.) 67 (10) (2015) 2262–2270.
[10] G. Laplanche, A. Kostka, O.M. Horst, G. Eggeler, E.P. George, Microstructure evolution and critical stress for twinning in the CrMnFeCoNi high-entropy alloy, Acta Mater. 118 (2016) 152–163.
[11] E.S.A. Podolskiy, Y. Shapovalov, E. Tabachinkova, A.S. Tortika, M.A. Tikhonovsky, B. Joni, É. Ódor, T. Ungar, S. Maier, C. Rentenberger, M. Zehetbauer, Anomalous evolution of strength and microstructure of high entropy alloy CoCrFeNiMn, after high pressure torsion at 300 and 77 K,, Adv. Eng. Mater. 22 (1) (2020) 1900752.
[12] I. Gutierrez-Urrutia, D. Raabe, Grain size effect on strain hardening in twinning-induced plasticity steels, Scripta Mater. 66 (12) (2012) 992–996.
[13] A.J. Zaddach, C. Niu, C.C. Koch, D.L. Irving, Mechanical properties and stacking fault energies of NiFeCrCoMn high-entropy alloy, JOM (J. Occup. Med.) 65 (12) (2013) 1780–1789.
[14] S. Huang, W. Li, S. Lu, F. Tian, J. Shen, E. Holmström, L. Vitos, Temperature dependent stacking fault energy of FeCrCoNiMn high entropy alloy, Scripta Mater. 108 (2015) 44–47.
[15] Z.J. Zhang, M.M. Mao, J. Wang, B. Gludovatz, Z. Zhang, S.X. Mao, E.P. George, Q. Yu, R.O. Ritchie, Nanoscale origins of the damage tolerance of the high-entropy alloy CrMnFeCoNi, Nat. Commun. 6 (1) (2015) 1–6.
[16] B. Schuh, F. Mendez-Martin, B. Völker, E.P. George, H. Clemens, R. Pippan, A. Hohenwarter, Mechanical properties, microstructure and thermal stability of a nanocrystalline CoCrFeMnNi high-entropy alloy after severe plastic deformation, Acta Mater. 96 (2015) 258–268.
[17] M. Tikhonovsky Stepanov, N. Yurchenko, D. Zyabkin, M. Klimova, S. Zherebtsov, A. Efimov, G. Salishchev, Effect of cryo-deformation on structure and properties of CoCrFeNiMn high-entropy alloy, Intermetallics 59 (2015) 8–17.
[18] Z. Li, S. Zhao, S.M. Alotaibi, Y. Liu, B. Wang, M.A. Meyers, Adiabatic shear localization in the CrMnFeCoNi high-entropy alloy, Acta Mater. 151 (2018) 424–431.
[19] S. Praveen, H.S. Kim, "High-Entropy Alloys: potential candidates for high-temperature applications–An Overview, Adv. Eng. Mater. 20 (1) (2018) 1700645.
[20] P. Chen, C. Lee, S.Y. Wang, M. Seifi, J.J. Lewandowski, K.A. Dahmen, H. Jia, X. Xie, B. Chen, J.W. Yeh, C.W. Tsai, Fatigue behavior of high-entropy alloys: a review, Sci. China Technol. Sci. 61 (2) (2018) 168–178.
[21] E.P. George, D. Raabe, R.O. Ritchie, High-entropy alloys, Nat. Rev. Mater. 4 (8) (2019) 515–534.
[22] Y.Z.Z. Tian, S.J.J. Sun, H.R.R. Lin, Z.F.F. Zhang, Fatigue behavior of CoCrFeMnNi high-entropy alloy under fully reversed cyclic deformation, J. Mater. Sci. Technol. 35 (3) (2019) 334–340.
[23] Y.K. Kim, G.S. Ham, H.S. Kim, K.A. Lee, High-cycle fatigue and tensile deformation behaviors of coarse-grained equiatomic CoCrFeMnNi high entropy alloy and unexpected hardening behavior during cyclic loading, Intermetallics 111 (2019) 106486.
[24] K.V.S. Thurston, B. Gludovatz, A. Hohenwarter, G. Laplanche, E.P. George, R. O. Ritchie, Effect of temperature on the fatigue-crack growth behavior of the high-entropy alloy CrMnFeCoNi, Intermetallics 88 (2017) 65–72.
[25] J.H. Kim, K.R. Lim, J.W. Won, Y.S. Na, H.S. Kim, Mechanical properties and deformation twinning behavior of as-cast CoCrFeMnNi high-entropy alloy at low and high temperatures, Mater. Sci. Eng., A 712 (2018) 108–113.
[26] Z. Tang, T. Yuan, C.-W.W. Tsai, J.-W.W. Yeh, C.D. Lundin, P.K. Liaw, Fatigue behavior of a wrought Al0.5CoCrCuFeNi two-phase high-entropy alloy, Acta Mater. 99 (2015) 247–258.
[27] M. Delshadmanesh, G. Khatibi, M.Z. Ghomsheh, M. Lederer, M. Zehetbauer, H. Danninger, Influence of microstructure on fatigue of biocompatible β-phase Ti-45Nb, Mater. Sci. Eng., A 706 (2017) 83–94.
[28] W.C. Oliver, G.M. Pharr, An improvved techniques for determining Hardness and elastic modulus using load and displacement sensing indentation experiments, J. Mater. Res. 7 (1992) 1564–1583.
[29] K. Alagarsamy, A. Fortier, M. Komarasamy, N. Kumar, A. Mohammad, S. Banerjee, H.C. Han, R.S. Mishra, Mechanical properties of high entropy alloy Al0.1CoCrFeNi for peripheral vascular stent application, Cardiovasc. Eng. Technol. 7 (4) (2016) 448–454.
[30] R. Newell, Z. Wang, I. Arias, A. Mehta, Y. Sohn, S. Florczyk, Direct-contact cytotoxicity evaluation of CoCrFeNi-based multi-principal element alloys, J. Funct. Biomater. 9 (4) (2018).
[31] M.A. Hemphill, T. Yuan, G.Y. Wang, J.W. Yeh, C.W. Tsai, A. Chuang, P.K. Liaw, Fatigue behavior of Al 0.5CoCrCuFeNi high entropy alloys, Acta Mater. 60 (16) (2012) 5723–5734.
[32] Y. Zhang, T.T. Zuo, Z. Tang, M.C. Gao, K.A. Dahmen, P.K. Liaw, Z.P. Lu, Microstructures and properties of high-entropy alloys, Prog. Mater. Sci. 61 (2013) (2014) 1–93.
[33] S. Stanzl-Tschegg, "Ultrasonic Fatigue," *Encyclopedia Of Materials: Science And Technology*, second ed., Elsevier, 2001, pp. 9444–9449.
[34] P. Bajons, K. Kromp, W. Kromp, H. Langer, B. Weiss, R. Stickler, Ultrasonic fatigue testing method - its practical application, Ultrason. Int. Conf. Proc. (1975) 95–101.
[35] R. Ebara, "The present situation and future problems in ultrasonic fatigue testing - mainly reviewed on environmental effects and materials' screening, Int. J. Fatig. 28 (11) (2006) 1465–1470.
[36] B. Guennec, A. Ueno, T. Sakai, M. Takanashi, Y. Itabashi, Effect of loading frequency in fatigue properties and micro-plasticity behavior of JIS S15C low carbon steel, in: 13th Int. Conf. Fract. 2013, ICF 2013, vol. 3, 2013, pp. 1906–1915.
[37] M. Papakyriacou, H. Mayer, C. Pypen, H. Plenk, S. Stanzl-Tschegg, Influence of loading frequency on high cycle fatigue properties of b.c.c and h.c.p. metals, Mater. Sci. Eng., A 308 (1–2) (2001) 143–152.
[38] S. Shao, M.M. Khonsari, J. Wang, N. Shamsaei, N. Li, Frequency dependent deformation reversibility during cyclic loading, Mater. Res. Lett. 6 (7) (2018) 390–397.
[39] Q. Chen, N. Kawagoishi, Q.Y. Wang, N. Yan, T. Ono, G. Hashiguchi, Small crack behavior and fracture of nickel-based superalloy under ultrasonic fatigue, Int. J. Fatig. 27 (10–12) (2005) 1227–1232.
[40] M. Klesnil, P. Lukác, Fatigue of Metallic Materials, second ed., vol. 71, Elsevier Science, 1992.
[41] C.R. Sohar, A. Betzwar-Kotas, C. Gierl, B. Weiss, H. Danninger, Gigacycle fatigue behavior of a high chromium alloyed cold work tool steel, Int. J. Fatig. 30 (7) (2008) 1137–1149.
[42] S. Kovacs, T. Beck, L. Singheiser, Influence of mean stresses on fatigue life and damage of a turbine blade steel in the VHCF-regime, Int. J. Fatig. 49 (2013) 90–99.
[43] M. Jane, L. Wagner, The very high cycle fatigue behaviour of Ti 6Al 4V alloy, Acta Phys. Pol. 128 (4) (2015) 497–502.
[44] K. Tokaji, K. Ohya, H. Kariya, Subsurface fatigue crack initiation in beta titanium alloys, Fatig. Fract. Eng. Mater. Struct. 23 (9) (2000) 759–766.
[45] A. Wan, J. Xiong, "Effect of stress ratio on HCF and VHCF properties at temperatures of 20 °C and 700 °C for nickel-based wrought superalloy GH3617M, Chin. J. Aeronaut. 32 (9) (2019) 2199–2210.
[46] American Society for Metals, ASM Handbook Vol. 2: Nonferrous Alloys and Special-Purpose Materials, Taylor & Francis, 1990, ISBN 978-0-87170-378-1, https://doi.org/10.31399/asm.hb.v02.9781627081627.
[47] P. Lukáš, L. Kunz, L. Navrátilová, O. Bokůvka, Fatigue damage of ultrafine-grain copper in very-high cycle fatigue region, Mater. Sci. Eng., A 528 (22–23) (2011) 7036–7040.
[48] S.E. Stanzl-Tschegg, Influence of material properties and testing frequency on VHCF and HCF lives of polycrystalline copper, Int. J. Fatig. 105 (2017) 86–96.
[49] G. Khatibi, J. Horky, B. Weiss, M.J. Zehetbauer, CHigh cycle fatigue behaviour of copper deformed by high pressure torsion, Int. J. Fatig. 32 (2) (2010) 269–278.
[50] S.J. Sun, Y.Z. Tian, H.R. Lin, H.J. Yang, X.G. Dong, Y.H. Wang, Z.F. Zhang, Transition of twinning behavior in CoCrFeMnNi high entropy alloy with grain refinement, Mater. Sci. Eng., A 712 (2018) 603–607.
[51] A.S. Hamada, L.P. Karjalainen, J. Puustinen, Fatigue behavior of high-Mn TWIP steels, Mater. Sci. Eng., A 517 (1–2) (2009) 68–77.
[52] C. Haase, L.A. Barrales-Mora, Influence of deformation and annealing twinning on the microstructure and texture evolution of face-centered cubic high-entropy alloys, Acta Mater. 150 (2018) 88–103.
[53] M.A. Meyers, Y.B. Xu, Q. Xue, M.T. Pérez-Prado, T.R. McNelley, Microstructural evolution in adiabatic shear localization in stainless steel, Acta Mater. 51 (5) (2003) 1307–1325.
[54] J.J. Roa, G. Fargas, J. Calvo, E. Jiménez-Piqué, A. Mateo, Plastic deformation and damage induced by fatigue in TWIP steels, Mater. Sci. Eng., A 628 (2015) 410–418.
[55] L.P. Karjalainen, A. Hamada, R.D.K. Misra, D.A. Porter, Some aspects of the cyclic behavior of twinning-induced plasticity steels, Scripta Mater. 66 (12) (2012) 1034–1039.
[56] S.J. Sun, Y.Z. Tian, H.R. Lin, X.G. Dong, Y.H. Wang, Z.J. Zhang, Z.F. Zhang, Enhanced strength and ductility of bulk CoCrFeMnNi high entropy alloy having fully recrystallized ultrafine-grained structure, Mater. Des. 133 (2017) 122–127.
[57] S.J. Sun, Y.Z. Tian, H.R. Lin, S. Lu, H.J. Yang, Z.F. Zhang, Modulating the prestrain history to optimize strength and ductility in CoCrFeMnNi high-entropy alloy, Scripta Mater. 163 (2019) 111–115.